Mechanical and thermal properties of carbon-based low-dimensional materials

Abigail L. Eaton, Marco Fielder, and Arun K. Nair*

Carbon-based low-dimensional materials possess many properties that make their implementation in nanodevices a subject of great interest. With these impressive transport and mechanical properties, one such use includes its use as a component of a Cu-based electrode. To investigate the applicability of a carbon chain (carbyne) in comparison to other carbon allotropes, including cyclo[18]carbon-carbyne hybrids and encapsulation inside a nanotube, we use multiscale computational methods to determine the mechanical and thermal properties of each structure. Under isolation carbyne requires the largest force to fracture and presents the highest thermal conductivity, whereas the hybrid structures have a lower thermal conductivity and break under a lower tensile force at the same strain as carbyne with unraveling mechanisms dependent on the number of cyclo[18]carbon included. For use in Cu electrodes, we find that carbyne also gives higher thermal conductivity when compared to other structures.

Impact statement

Carbon-based low-dimensional materials exist as chains and rings at the nanoscale that have great potential for application in nanodevices. However, some of these nanoscale structures are reactive on substrates and lose their properties. We investigate the mechanical and thermal properties of the low-dimensional structures of a chain of carbon atoms known as carbyne, carbyne and cyclo[18]carbon hybrids, and encapsulation of these inside carbon nanotubes to test their stability on Cu(111) substrate acting as an electrode. The carbyne and cyclo[18] carbon hybrids are found to display high mechanical properties during tensile studies, and cyclo[18]carbon is determined to be able to withstand higher strains. The deformation mechanisms of cyclo[18]carbon hybrids at different strains are also uncovered. An isolated carbyne chain was found to have the highest thermal and mechanical properties of the structures investigated, which is further established on a Cu substrate compared to other low-dimensional structures studied here.

Introduction

Low-dimensional materials, specifically those composed of carbon, are a subject of high interest due to their impressive mechanical properties and comparably small masses. This classification includes nanomaterials such as carbyne, graphene, and carbon nanotubes (CNTs). Carbyne, the smallest known nanofiber, is a one-dimensional chain of *sp*-hybridized carbon atoms that occurs in a polyynic structure with alternating single and triple bonds (≡C–C≡C–)n or with a cumulenic structure consisting of all double bonds (=C=C=)n.[1] Despite its reactive structure, it has been discovered naturally occurring in interstellar dust and meteorites.[2,3] It is of great importance to the future of nanomaterials, as it displays high mechanical performance, including a specific strength of 7.5×10^7 N·m/kg and specific stiffness of approximately 10^9 N m/kg that rivals those of graphene and carbon nanotubes.[1] Among these is also an impressive Young's modulus of 3 TPa.[4] Such properties suggest that the chain would be ideal for applications requiring high mechanical demands with limited material volume. Some potential implementations include nanosprings and use in metal-matrix nanocomposites.[5,6] The low-dimensional carbon chain also exhibits excellent thermal characteristics and is reported to have a high thermal conductivity.[7,8] The tunable thermal properties and thermal conductivity that is comparable to that of existing nanowires imply success of the chain for mechanical/thermal energy storage.[9] However, synthesis of the chain remains a challenge due to its instability. This has been addressed with current methods of encapsulating the chain in single or multiwalled CNTs[10,11] and the use of carbyne in metal-matrix nanocomposites.[6]

Abigail L. Eaton, Multiscale Materials Modeling Lab, Department of Mechanical Engineering, University of Arkansas, Fayetteville, USA
Marco Fielder, Multiscale Materials Modeling Lab, Department of Mechanical Engineering,University of Arkansas, Fayetteville, USA
Arun K. Nair, Multiscale Materials Modeling Lab, Department of Mechanical Engineering, University of Arkansas, Fayetteville, USA; Institute for Nanoscience and Engineering, University of Arkansas, Fayetteville, USA; nair@uark.edu
*Corresponding author
doi:10.1557/s43577-022-00325-2

Another low-dimensional carbon allotrope is cyclo[18] carbon (C18); a highly reactive ring of 18 carbon atoms that displayed polyynic bonding during its initial synthesis during an atom manipulation study.[12] With a specific stiffness and a Young's modulus that are lower than those of carbyne, in addition to the ring's critical strain of 32 percent and comparable specific tensile strength, it has been proposed for nanomechanical applications as an ultra-elastic molecular O-ring in a study by Fang and Hu.[13] When C18 was connected to two carbon chains by Zhang et al., the structure also exhibited high conductance in comparison to other samples tested with a C18 ring of both polyynic and cumulenic structures.[14] However, further studies are needed for an in-depth understanding of this structure, including its response to tensile strain until fracture and thermal conductivity. The impressive attributes of C18 and carbyne inspire the need for an investigation of the thermal transport and mechanical properties of C18-carbyne structures. Specifically, its potential application in nanodevices as opposed to carbyne and other carbon-based low-dimensional materials is of interest, including the addition of CNT for encapsulation of carbyne. These hybrids may have thermal and mechanical properties that could further advance nanodevice applications.

Using molecular dynamics (MD) and density functional theory (DFT) methods, we study the tensile and thermal properties of carbyne, C18, carbyne with varying rings of C18, and carbyne capped in a CNT to determine the possibility of carbyne applications requiring high thermal conductivity and mechanical characteristics. We determine the transforming and breaking forces with corresponding strains for all samples under tensile loading. Thermal studies are then conducted to calculate the thermal conductivity of the samples at room temperature and as an electrode on a Cu substrate.

Materials and methods

Materials

We study the mechanical properties of carbyne, *n*C18-carbynes ($n = 1$, 2, and 3 rings), capped CNTs, and their thermal properties on a Cu substrate, using MD and DFT methods. The large-scale atomic/molecular massively parallel simulator (LAMMPS)[15] is utilized with a ReaxFF force field designed for modeling of C/H/O materials and Cu for the MD studies.[16] The validity of this force field is reinforced by comparison of the strain energy calculation for C18 for strains of −20 to 20 percent using MD and DFT. This is discussed in the "Tensile and compressional strain energy of C18" section, following a previous study.[13] We use MD method on all samples to perform thermal testing and tensile studies, which are conducted using the steered molecular dynamics (SMD) method.[17] The samples of interest, which include a chain of cumulenic carbyne, a cumulenic C18 ring, *n*C18-carbyne with 1–3 rings, and a capped (5, 5) CNT with and without encapsulated carbyne, are shown in **Figure 1**. All chains are approximately 80 Å long, and the capped CNT is nearly 100 Å in length. The sliced Cu(111) substrate, which is used for initial analysis of the carbon-based structures as electrodes, may be seen in Figure 1g with a chain of carbyne capped using graphene sheets, and in Figure 1h with carbyne encapsulated in the CNT after being equilibrated at 300 K using a canonical (NVT) ensemble. Another Cu(111) block structure is also studied with low-dimensional materials as shown in Figure 1i–j;

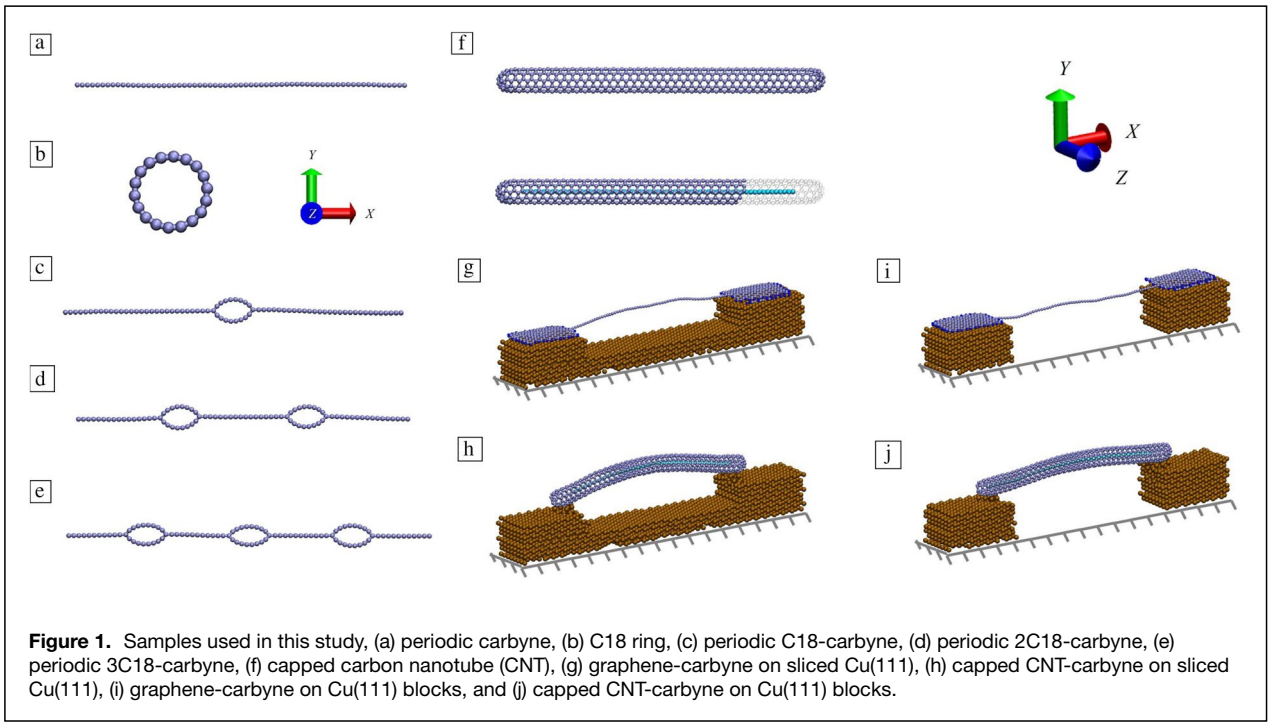

Figure 1. Samples used in this study, (a) periodic carbyne, (b) C18 ring, (c) periodic C18-carbyne, (d) periodic 2C18-carbyne, (e) periodic 3C18-carbyne, (f) capped carbon nanotube (CNT), (g) graphene-carbyne on sliced Cu(111), (h) capped CNT-carbyne on sliced Cu(111), (i) graphene-carbyne on Cu(111) blocks, and (j) capped CNT-carbyne on Cu(111) blocks.

this structure eliminates the Cu base as seen in Figure 1g–h. The Cu sample dimensions are approximately 140 × 15 × 20 Å (excluding the gaps for samples in Figure 1g–j) in the *x*, *y*, and *z* dimensions, with a periodicity along the *z*-direction. All sample visualizations utilized VMD.[18] All carbon-based materials are generated using nanoengineer-1,[19] excluding the capped CNT, which was modeled using the NanoCap software.[20]

Tensile testing

The SMD tensile testing was carried out for samples a–f (Figure 1) in vacuum after equilibration at 10 K to avoid the effects of thermal vibration. We did perform a parametric study, and it was confirmed that the *n*C18-carbyne samples break at approximately the same force when the temperature ranges between 10 and 300 K. The breaking force of carbyne at 10 and 300 K has also been reported to vary approximately 1 nN in a previous tensile study for a chain length of 80 Å.[21] An atom (carbyne, C18, *n*C18-carbyne) or selection of atoms (CNT, CNT-carbyne) on the left-hand side of the sample have fixed boundary conditions, whereas the atom(s) on the right are pulled with a constant velocity of 0.05 m/s along the *x*-axis. In the case of the CNT structures, multiple atoms are attached to the spring used for the SMD calculations by LAMMPS for symmetry of force distribution and inclusion of the carbyne chain in the CNT-carbyne sample. Throughout pulling, the strain of the sample is recorded in relation to the spring force required to maintain the constant velocity, which we then use to determine the breaking or structure transformation force of each sample. Strain is calculated along the *x*-axis and is determined by the change in the length of the chain along the *x*-direction divided by the length of the unstrained chain. Virial stress is also recorded per atom as implemented in LAMMPS and has units of stress multiplied by cell volume.[22] For the purpose of this study, the carbyne cell volume is approximated using a 3.35 Å by 3.35 Å square cross-sectional area, which was used in a previous MD study,[23] and a cell length corresponding to the length of the chain as it undergoes strain. For the other *n*C18-carbyne samples, the cross section is altered to reflect a rectangular cross section of 3.35 Å by 7.39278 Å; the diameter of the C18 ring. The CNT area is modeled as a ring with a radius of 3.43 Å and thickness of 3.4 Å,[24] whereas the CNT-carbyne area is calculated as a circular cross section with a radius equivalent to the outer radius of the CNT ring. Observation and imaging of the stress distributions are performed using the visualization software, OVITO.[25]

Thermal studies

In this study, we use the Müller-Plathe reverse nonequilibrium method to compute the thermal conductivity, which is the rate of energy transfer in a material with a temperature gradient.[7,26] MD simulations are performed using an NVE ensemble, and kinetic energy is exchanged between atoms in a hot and cold reservoir to induce a temperature gradient. The cumulative energy transferred and the subsequent temperature gradient as the system approaches a steady state are measured. The thermal conductivity (κ) can then be computed using Fourier's Law, as seen in Equation 1 where J_0 is the heat flux, Q is heat flow rate, dE is the cumulative kinetic energy transferred, dt is the simulation time, A is the cross-sectional area, and dT/dx is the temperature gradient along the system length.[26]

$$\kappa = \frac{J_0}{\mathrm{d}T/\mathrm{d}x} = \frac{Q}{2A}\left(\frac{1}{\mathrm{d}T/\mathrm{d}x}\right) = \left(\frac{\mathrm{d}E}{\mathrm{d}t}\right)\frac{1}{2A}\left(\frac{1}{\mathrm{d}T/\mathrm{d}x}\right) \quad (1)$$

It should be noted that thermal conductivity is dependent on the cross-sectional area and for our studies, the cross-sectional area used for calculations is discussed in the "Materials" and "Tensile testing" sections.

For the thermal conductivity simulations of the carbon structures, the models are periodic in all directions and approximately 80 Å in length. To ensure system averaging, there are 10 chains for the carbyne and *n*C18-carbyne models. The CNT and CNT-carbyne models utilize three repeated structures due to the large number of atoms in the system. It should also be noted that, for the simulations which include the sliced Cu(111) or Cu(111) blocks, the *x* and *y* boundaries are not periodic and thus mimicking a nanodevice, hence the division by two in Equation 1 for periodic boundaries is not included. In this case, only one image of the sample is used due to the large number of atoms, and the cross-sectional area is calculated as the area of the Cu block across the gap (approximately 20 × 6 Å) added to the area of the carbon-based material suspended over it for the sliced Cu(111) samples. The models are first equilibrated using an NVT ensemble to a temperature of 300 K before the Müller-Plathe method is applied with the hot and cold reservoirs being approximately 20 Å in width. A timestep of 0.1 fs is used, and the exchange of kinetic energies between reservoirs occurs every 100 timesteps. The heat is exchanged for a simulation time of 20 ps. For the nonperiodic simulations, the individual atoms on either side of the carbon-based materials have a fixed boundary conditions (in the *x*-direction for carbyne and in *x* and *z* for C18-carbyne, CNT, and CNT-carbyne).

Tensile and compressional strain energy of C18

To validate the tensile studies and force values obtained and to find the specific stiffness of C18, we further investigate the compression and tensile properties of C18. The energy of the ring is calculated using DFT and MD (energy minimization) for strains of −20 to 20 percent. The DFT studies were conducted using Quantum ESPRESSO[27] with projected augmented wave (PAW) pseudopotentials[28] and PBE functional[29] for the carbon atoms. The C18 ring is modeled in a vacuum with a spacing of approximately 10 Å between periodic images. Structural relaxation calculations are carried out with a 1 × 1 × 1 k-point mesh and the employment of Grimme's DFT-D2 van der Waals correction for modeling of the C atom interactions.[30] The kinetic energy cutoff is set to 558 eV, and convergence is achieved when the difference in energy between calculation iterations is less than a threshold

of 1×10^{-6}. To find the lowest energy configurations corresponding to C18 strain variations between −20 and 20 percent, we apply fixed boundary conditions to diametrically opposite atoms with the strained diameter of the ring while the remaining atoms are free to move during relaxation. Once the relaxation is completed, the final energy of the system is computed along with the atomic positions and electron densities. The electron densities, which provide insight into the bonding structure of the ring, can be visualized as isosurfaces using VESTA.[31] To compare DFT and MD results, the energy of the C18 with strains between a compressional −20 percent and tensional 20 percent are normalized and the forces are computed and then compared.

Electron density of strained nC18-carbyne

We additionally validate the transformations occurring in the *n*C18-carbyne samples during the SMD tensile study. We conduct self-consistent field (SCF) calculations using Quantum ESPRESSO[27] for the *n*C18-carbyne samples at strain values leading up to the strain just prior to their first transformation determined from the SMD results. We extract the atom coordinates for the corresponding strains directly from the SMD simulations. The simulation box size is determined by the maximum strain of the longest 3C18-carbyne sample, for which there is a vacuum of ~10 Å between the periodicities. We then use these results to visualize the electron densities of the samples by slicing 2D planes through the rings of the chains using VESTA.[31]

Discussion and conclusion

Tensile testing results

The force and strain for all the samples are recorded throughout the SMD study. We find the force at which the samples initially undergo structural transformation (transforming force), and then determine the breaking (fracture) force with corresponding strains (see **Figure 2**a).

During the tensile studies, carbyne endures tensile strain due to the F_{xx} spring force before one of its bonds breaks at the point where the spring is attached at approximately 35 nN. The breaking force of carbyne has been reported as 9 nN from a tensile study for a similar length chain; however, this chain had a polyyne bonding structure.[4] It is possible the difference is due to the dissociation of the bonds of each structure; polyyne includes single C–C bonds while cumulene is composed of double bonds that would require a higher force to break. It should also be noted that the carbon-carbon bond at which the carbyne breaks is stretched from a C=C bond to a C–C bond, which may affect the pulling force. This occurs between a strain of approximately 14 and 14.6 percent and causes the steep increase of slope for the force-strain relationship of carbyne (see Figure 2a). Between these strain values, most bonds in the chain are extended from the length of a double to single carbon bond. An isolated C18 ring experienced multiple bond breaks that may be seen in the array of force peaks. This is due to the unraveling of the ring; rather than fracturing of a C–C bond as observed for the chain of C-atoms; the C-atoms start to undergo structural transformation from C18 to a carbon

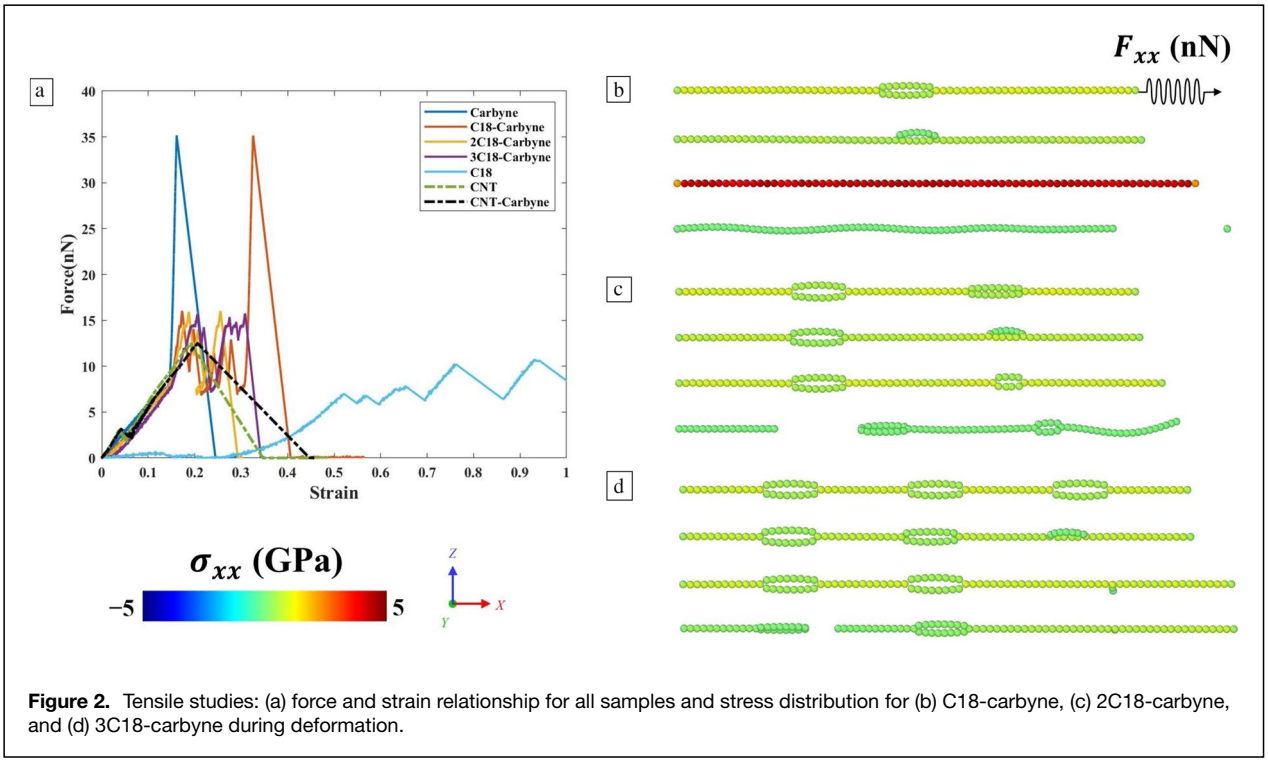

Figure 2. Tensile studies: (a) force and strain relationship for all samples and stress distribution for (b) C18-carbyne, (c) 2C18-carbyne, and (d) 3C18-carbyne during deformation.

chain. This process is repeated while the force is distributed through the ring to each atom prior to transformation. The initial peak force of the C18 ring, which led to its first structural change under tensile strain, is approximately 7 nN at 50 percent strain. This agrees with a tensile study completed by Fang and Hu, in which a critical force of 4.5 nN is reported for the single C18 ring and it is noted to not surpass a strain of 50 percent.[13] The CNT and CNT-carbyne structures fractured at a strain closer to that of the carbyne chain but at a force closer to that of the C18 at ~12.46 nN and 12.49 nN, respectively. These two samples don't have a higher tensile strength or ability to withstand high strains in comparison to the other structures.

A combination of breaking patterns observed in the carbyne and C18 may be seen in the *n*C18-carbyne samples depending on the number of rings in the chain. The sample with one ring experiences its first change at a transforming force of approximately 15 nN prior to unraveling into a chain of carbyne that breaks at 35 nN. This may be noted with the two peaks associated with this sample in Figure 2a and the process visualized in Figure 2b. Unlike this sample, the chains with 2 and 3 C18 rings experience bond breaks prior to full carbyne transformation. As may be seen in Figure 2, the ring closest to the applied force starts to unravel first. However, before the ring is fully unraveled and while the second ring is unchanged, the chain breaks at a bond between the carbyne chain and C18 furthest from where the spring is attached. Upon further inspection, this is a single C–C bond with sp^3-hydridized C-atom bonding with the carbyne and C18 ring. This mechanism is also seen for the 3C18-carbyne sample; neither sample achieves the breaking force of 35 nN. As noted for the structural transformation of the sample with a single C18, these samples break at 15 nN.

From these relationships, it can be inferred that the inclusion of the C18 rings in the carbon chains are not ideal for increasing the tensile strength of the carbyne. All low-dimensional samples, excluding the isolated C18 ring, break or transform at a strain of approximately 18 percent, which coincides with a previous study's report for the critical strain of carbyne of 18–19 percent.[1] The use of C18 did not increase the critical strain of carbyne despite the impressive elastic properties of the isolated carbon ring. While the single C18-carbyne sample delays the fracturing of the chain, it requires a transformation between the C18-carbyne structure to a linear carbon chain before achieving the strength of the chain post-transformation. However, due to this change from the ring structure to a carbon chain, the ultimate failure strain of the single C18-carbyne structure is higher than that of the carbyne chain.

The stress distribution in the *n*C18-carbyne provides an insight into the tensile properties of these chains. These may be seen in Figure 2b–d, which show the structure before and after the initial unraveling of the rings and breaking of the chains. The C18-carbyne shows a gradual increase in stress during the tensile test before the distribution of stress changes in the ring; one half (bottom portion of the ring) continues to increase while the top portion releases some of the stress after the first bond breaks. Then, after the ring has unraveled, the stress of the carbyne chain approaches 5 GPa before the chain also breaks and stress in the chain is released. 2C18-carbyne and 3C18-carbyne do not reach this 5 GPa stress value prior to fracture in the samples; they break at approximately 1 GPa. After their first C18 ring unravels, the chains break at a carbyne and C18 intersecting bond. This pattern may be occurring due to the single C–C bonds in the structure at this point being not as strong as a double bond that must break for carbyne. The weak bonding, combined with the uneven distribution of stress between the chain (higher stress) and C18 ring (lower stress), results in these chain fracturing at a lower force than carbyne under tensile loading.

To validate the force values under tensile testing using MD, we use DFT to find the ground-state energies and compute the forces at different strains. We pick the C18 sample for this test as it has the lower number of atoms and is thus computationally less expensive. Moreover, the specific stiffness of C18 needs to be determined. By using DFT and MD methods we find the strain energies at 0 percent strain and at tension and compression strains of 2, 4, 10, 15, and 20 percent. After normalization of the energy values, both methods return similar strain energies that may be seen in **Figure 3**a, which serves to further validate the force field used.

The charge density of the unstrained and strained samples is visualized in the form of isosurfaces denoted by their color for each density level between 0.1 and 0.4 $Å^{-3}$. These densities are indicative of the bonding structure of the rings; the charge densities between atoms implies it is a cumulenic structure. As may be seen in Figure 3a, the charge density of 0.3 $Å^{-3}$ remains constant for all strained samples; they are all cumulenic with double C=C bonds. This bonding is not affected by the strain due to the strain range used; the critical strain for C18 has been reported as 32 percent.[13] All strains studied in this paper fall within the elastic range of the C18.

Given the strain energies, it is possible to calculate the specific stiffness for the C18 ring following the method detailed by Muller and Nair.[6] For the MD and DFT methods, the specific stiffness is determined to be 6.32 GPa cm^3/g and 9.79 GPa cm^3/g, respectively. This value is much lower than that of carbyne, which has been reported to have a specific stiffness of 673 GPa cm^3/g.[6] Carbyne has also been noted to have a specific stiffness that is twice that of CNTs and graphene;[1] the specific stiffness of C18 is also lower than these materials. This is to be expected, as the C18 is able to withstand a higher strain than carbyne and has more modes of transformation during tensile pulling than a one-dimensional chain. By comparing the forces obtained from MD and DFT, we note that the maximum difference at 20 percent and −20 percent are 0.37 nN and 0.31 nN, respectively. This may be attributed to the difference between the van der Waals interactions for DFT calculations in comparison to the ReaxFF force field used

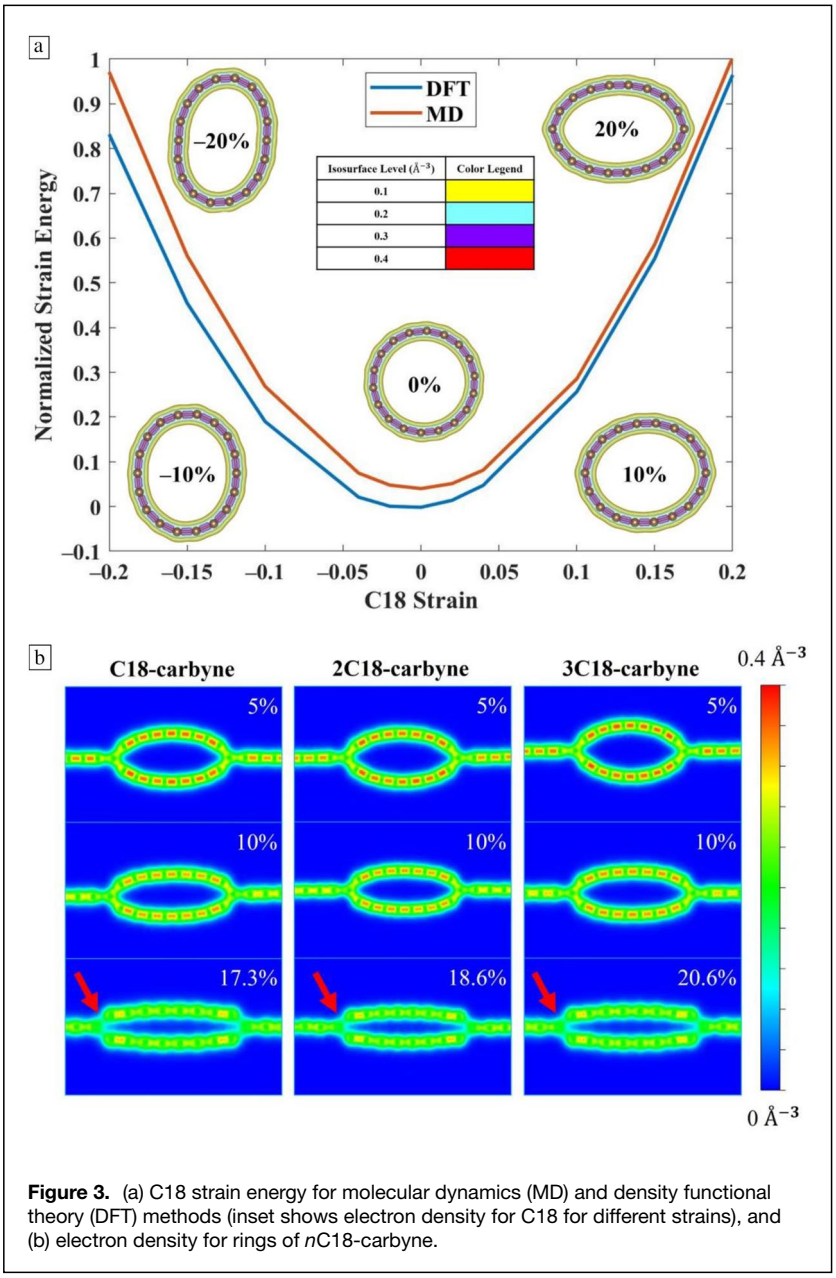

Figure 3. (a) C18 strain energy for molecular dynamics (MD) and density functional theory (DFT) methods (inset shows electron density for C18 for different strains), and (b) electron density for rings of *n*C18-carbyne.

for MD. However, the differences are low, verifying the SMD force calculations.

To further validate the results of the SMD simulations, we also study the electron density of the *n*C18-carbyne samples at strains of 5 percent, 10 percent, and the transforming strain corresponding to each sample. For C18-carbyne, 2C18-carbyne, and 3C18-carbyne, these strains are respectively 17.3, 18.6, and 20.6 percent. The progression for each may be seen in Figure 3b for the right-most ring of each hybrid chain, as this is where the first transformation occurs. With an increase in strain, we note a decrease in electron density in the bonds at which the C18 and carbyne intersect denoted by a red arrow in Figure 3b, indicating this bond is stretched more compared to surrounding bonds. This concurs with the SMD results, in which we see the transformations first occurring at this intersection for all *n*C18-carbyne samples.

Thermal studies results

Beyond the tensile properties of the carbyne and C18 structures, their ability to conduct heat also impacts their applicability in nanodevices. Thus, we use the Müller-Plathe reverse nonequilibrium method to determine the thermal conductivity of all samples excluding C18 with periodic boundaries, and the results are shown in **Figure 4**a. For a more in-depth understanding, the number of vibration modes during the thermal simulations are also identified. These vibration modes are important to study, as they relate to the longitudinal and transverse acoustic modes of the chains and the transport of thermal energy via phonon modes.

Comparing all structures, the carbyne exhibits the highest thermal conductivity at 300 K as approximately 0.05 kW/m K, which agrees with a previous study.[7] A comparison between the thermal conductivity values we calculate for carbyne and those from literature can be found in Section S1 of the Supplementary Materials. Deng and Cranford found that carbyne had a higher thermal conductivity relative to its atomic weight when compared to a (5, 5) CNT and graphene.[7] Its low-dimensional status and short length also potentially result in the single vibration mode noted for this sample in Figure 4b, which may be influencing the comparably high thermal conductivity.[8] Though the C18 ring also has impressive transport properties, their addition to the carbyne chains did not increase the system's thermal conductivity. The *n*C18-carbyne samples all display similar κ values, which are less than half that of carbyne with the same chain length. Their number of vibrational modes, seen in Figure 4c–e for the *x*–*y* plane, are also proportional to the number of rings used. The thermal conductivity of the CNT structure, which experiences a single visible vibration mode in the *x*–*y* plane, is calculated as 0.018 kW/m K. This is within range of a previous study completed for various lengths of single walled CNTs for lengths of 50 and 100 Å.[32] Encapsulating a chain of cumulene in the CNT did not increase the structure's thermal conductivity as expected, though CNT-carbyne also only experiences one visible vibration mode (Figure 4g). This is assumed to be due to interaction occurring between the carbyne chain and

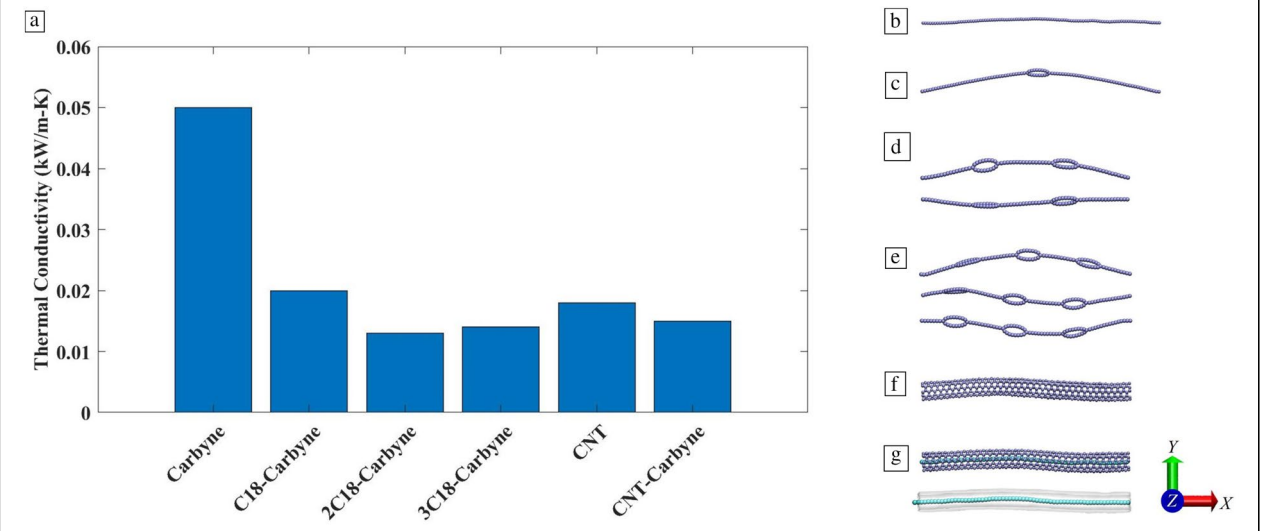

Figure 4. (a) Thermal conductivity of carbon-based structures for periodic case in vacuum and vibration modes for (b) carbyne, (c) C18-carbyne, (d) 2C18-carbyne, (e) 3C18-carbyne, (f) carbon nanotube (CNT), and (g) CNT-carbyne.

CNT that disrupts the linear transport noted for an isolated carbyne.

Next, a Cu(111) substrate is introduced to mimic the setup of an electrode,[14] in which carbyne-based samples could be placed to study the thermal conductivity for the chain of cumulenic carbyne, C18-carbyne, CNT, and CNT-carbyne. These Cu substrate structures do not include 2C18-carbyne and 3C18-carbyne because they were determined to have similar thermal conductivity values to C18-carbyne (see Figure 4a). Stability of the C18 and C18-carbyne on the Cu(111) surface is shown in Section S2 of the Supplementary Materials. The thermal conductivity of a Cu(111) block, which was used to determine the effect of a substrate on the carbon-based samples while acting as an electrode base, may be seen in **Figure 5**a–b. This is validated in Section S1 of the Supplementary Materials. The addition of carbyne, C18-carbyne, CNT, and CNT-carbyne on the sliced Cu surface (see Cu(111) structure in Figure 5a) minimally increased this value. However, it should be noted that graphene sheets were added to the end of the carbyne and C18-carbyne chains to ensure that they remained on the Cu surface with a periodicity along the *z*-axis. Our SMD study confirmed that an isolated carbyne and graphene-carbyne have a similar breaking force and response to tensile testing.

We determine that the results for the sliced Cu(111) structures are similar in value to the thermal conductivity of Cu due to the effect of the metal (Cu) spanning the gap where heat exchange occurs and the contribution of its cross-sectional area for thermal conductivity calculations. To mitigate this effect, we use the Cu(111) block structure as shown in Figure 5b. With this Cu block structure, we note an increase in thermal conductivity for all samples due to the presence of low-dimensional materials. As with the periodic case, the copper sample consisting of carbyne has the highest thermal conductivity of 0.24 kW/m K. In comparison, Cu-CNT-carbyne has the lowest thermal conductivity of 0.052 kW/m K. We contribute the variance in thermal conductivity values between samples to the simulation boundaries of nonperiodic compared to periodic and vibrational modes. Periodic systems lead to ballistic transport of phonons against the direction of imposed heat transfer, which reduces the measured temperature gradient and in turn the thermal conductivity.[33]

Deng and Cranford[7] report that carbyne has a high thermal conductivity and only two acoustic phonon modes in which heat travels as compared to other low-dimensional materials such as graphene. Carbyne is noted to have longitudinal and out-of-plane transverse modes, for which the vibrational modes correspond with movement in the *x*- and *y*-axes in our study, respectively. Of the limited number of modes, the out-of-plane transverse mode is theorized to be the most important by Deng and Cranford, allowing high thermal conductivity along the axis of the chain. These modes may be seen in the vibration of the chain in the inset of Figure 5a–b.

We observe the next highest thermal conductivity in Cu-C18-carbyne, for which we observe an additional in-plane vibrational mode with the C18 ring (see Figure 5c). This mode could be contributing to the lower thermal conductivity, which has been noted for graphene. Though the out-of-plane transverse mode is considered a large component of the thermal conductivity of graphene by Lindsay et al.,[34] the 2D material has three acoustic phonon modes. As noted by Wang and Lin,[8] the presence of more phonon modes could cause overlapping and phonon–phonon scattering that reduces

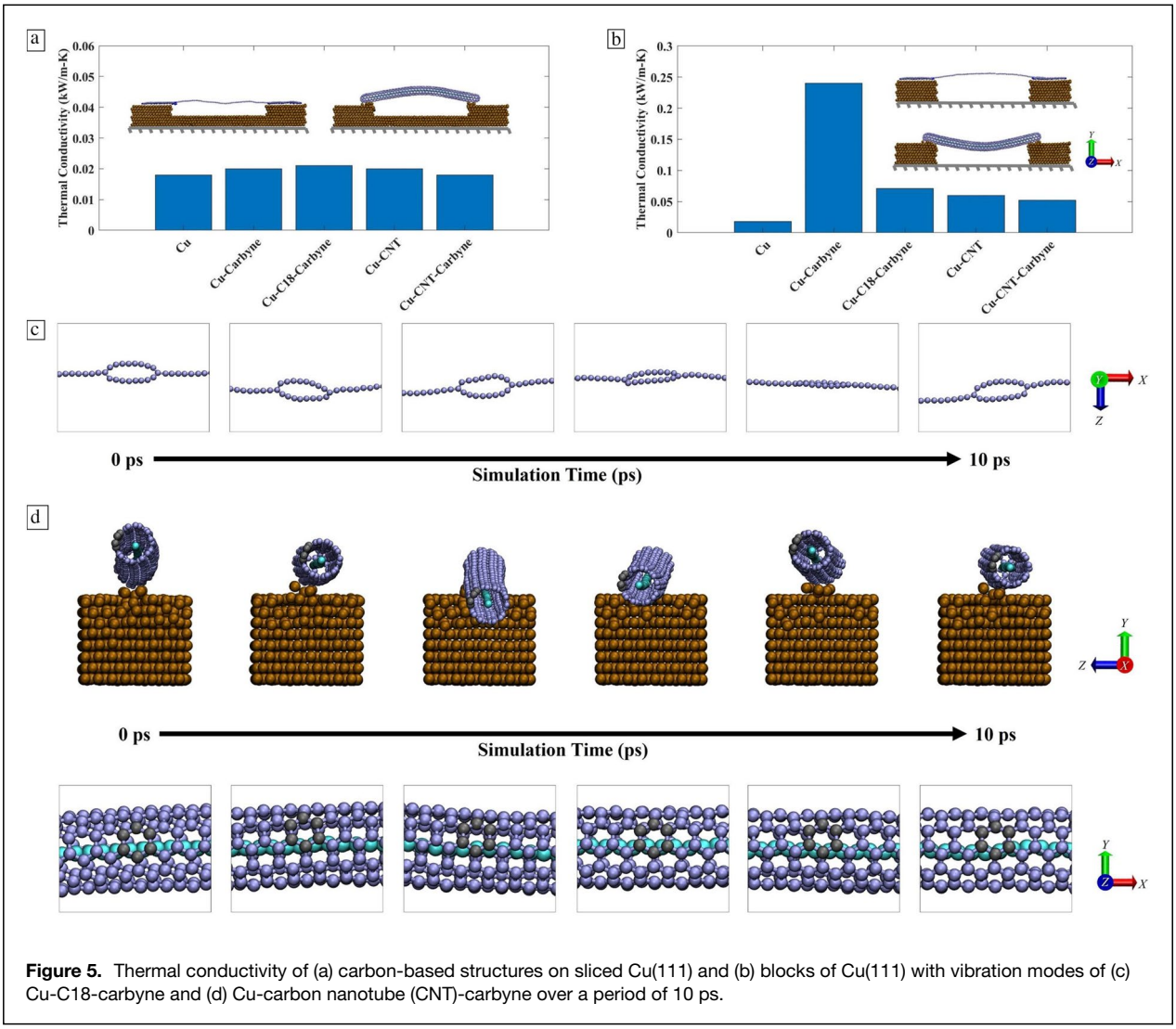

Figure 5. Thermal conductivity of (a) carbon-based structures on sliced Cu(111) and (b) blocks of Cu(111) with vibration modes of (c) Cu-C18-carbyne and (d) Cu-carbon nanotube (CNT)-carbyne over a period of 10 ps.

thermal conductivity. It is possible that this is occurring in the Cu-C18-carbyne structure. This may be the case for the CNT-carbyne structures as well, as they have the same bonding structure as graphene.

To further investigate the vibration modes occurring in the CNT samples during the thermal simulations, we study Cu-CNT-carbyne over a period of 10 ps. As opposed to carbyne, which has been reported to include two vibration modes (out-of-plane transverse and longitudinal), graphene includes a third in-plane transverse mode.[7] This, combined with its three-dimensional structure, requires a more in-depth analysis of the CNT structures throughout the thermal simulations. The out-of-plane transverse mode of carbyne results in vibrations along the *y*-axis. For the CNT structures, the out-of-plane vibration mode results in vibration in both the *y*-axis and *z*-axis. This may be seen in Figure 5d, in which the CNT-carbyne rotates around the *x*-axis.

To observe the in-plane modes of the CNT structures, we focus on a single hexagonal section of the tube denoted by grey atoms in Figure 5d over the same time period. We observe changes in bond lengths and bond bending occurring in the hexagon that is contributed by the in-plane vibration mode, as this mode is tangential to the CNT surface.

For comparison, we plot the thermal conductivity calculated for the periodic cases and nonperiodic Cu(111) block samples (Figure 5b) with the corresponding structural transforming force determined using tensile tests in **Figure 6**. The relationship between the thermal conductivities and tensile breaking forces of the carbon-based materials is indicative of their adaptability for use in applications, such as nanodevices, requiring high tensile strength and an ability to conduct heat. We find that carbyne, in a periodic or nonperiodic boundary when placed on Cu(111) blocks, has the highest transforming/breaking force and thermal conductivity when compared to

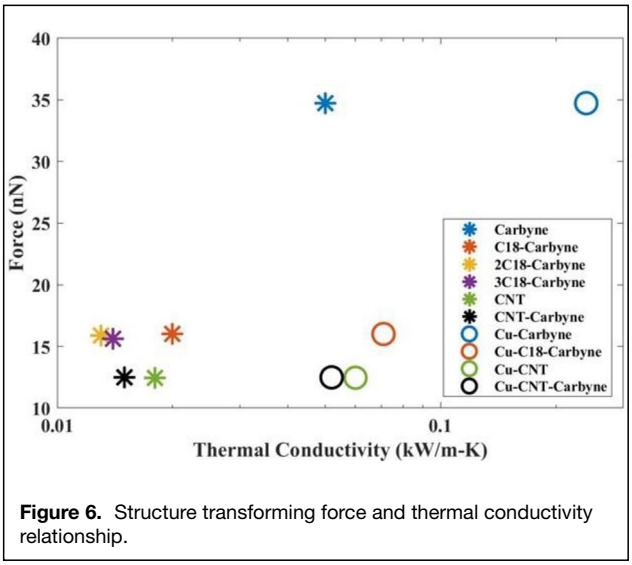

Figure 6. Structure transforming force and thermal conductivity relationship.

the other samples. The C18-carbyne samples have the second highest structure transforming force and thermal conductivity.

Conclusion

The mechanical and thermal properties of several carbon-based materials, including carbyne, C18, *n*C18-carbynes, and CNTs with and without encapsulated carbyne, were investigated using MD and DFT methods. During the tensile study, carbyne exhibited the highest force of approximately 35 nN prior to breaking under a tensile strain of 18 percent. The *n*C18-carbyne chains were found to break and transform at the same strain as the chain of carbyne at lower forces; they are not ideal for applications requiring an ability to withstand high strain or tensile strength. Additionally, varying the number of rings on the chains was not shown to greatly impact the samples' breaking force or thermal conductivity, though the chain with a single ring was noted to unravel into a chain of carbyne. This may be an interesting property to explore for applications where more deformation is needed at low strains while maintaining an ability to have a high strength at higher strains. Carbyne and C18 excel in different aspects; whereas carbyne resulted in the highest breaking force and thermal conductivity, C18 withstood a higher strain. Additionally, we determine the specific stiffness of C18 to be approximately 6.32–9.79 GPa cm^3/g, which is lower than the value reported for carbyne.

The ability of carbyne to withstand the highest tensile breaking force, compounded with its thermal conductivity of 0.05 kW/m K with periodic boundaries, make it an ideal material for use in nanodevices. This is further noted for the Cu-carbyne structure Cu(111) blocks, for which the thermal conductivity is ~5 × higher at 0.24 kW/m K compared to the Cu sliced case that is not periodic along the *x*-axis, which indicates that the distance between low-dimensional material and Cu base affects the thermal conductivity. Thus, the use of carbyne as an electrode in nanodevices with Cu(111) surface may be preferable for high thermal conductance, compounded with its efficiency relative to its mass compared to the *n*C18-carbyne structures and CNT structures. Though the use of CNT to encapsulate and shield carbyne from reactive surfaces is beneficial in application, it decreases the thermal conductivity of the CNT-carbyne structure. The CNT structures would be better suited for applications where thermal insulation is desired rather than a better ability to dissipate thermal energy.

Acknowledgments

We acknowledge the support from the Arkansas High Performance Computing Center and gratitude to the University of Arkansas in the awarding of the Doctoral Academy Fellowship.

Funding

The authors would like to thank and acknowledge the support from the National Science Foundation (Grant No.1929244) for full funding of this research.

Data availability

The data are currently not available as they are used for future work.

Code availability

Software (LAMMPS and Quantum ESPRESSO) used in this study are opensource and cited in the "Materials and methods" section of the manuscript.

Conflict of interest

Authors declare they have no conflict of interest.

Ethical approval

Not applicable.

Consent to participate

Not applicable.

Consent for publication

Authors consent to the publication of this research.

Supplementary Information

The online version contains supplementary material available at https://doi.org/10.1557/s43577-022-00325-2.

References

1. M. Liu, V.I. Artyukhov, H. Lee, F. Xu, B.I. Yakobson, *ACS Nano* **7**(11), 10075 (2013)
2. A. Webster, *Mon. Not. R. Astron. Soc.* **192**(1), 7P (1980)
3. R. Hayatsu, R.G. Scott, M.H. Studier, R.S. Lewis, E. Anders, *Science* **209**(4464), 1515 (1980)
4. A.K. Nair, S.W. Cranford, M.J. Buehler, *Europhys. Lett.* **106**(3), 39901 (2014)
5. B. Faria, N. Silvestre, C. Bernardes, J.N.C. Lopes, *Physica E* **117**, 113831 (2020)
6. S.E. Muller, A.K. Nair, *Comput. Mater. Sci.* **159**, 187 (2019)

7. Y. Deng, S.W. Cranford, *Comput. Mater. Sci.* **129**, 226 (2017)
8. M. Wang, S. Lin, *Sci. Rep.* **5**, 18122 (2016)
9. X. Liu, G. Zhang, Y.-W. Zhang, *J. Phys. Chem. C* **119**(42), 24156 (2015)
10. S. Toma, K. Asaka, M. Irita, Y. Saito, *Surf. Interface Anal.* **51**(1), 131 (2019)
11. L. Shi, P. Rohringer, K. Suenaga, Y. Niimi, J. Kotakoski, J.C. Meyer, H. Peterlik, M. Wanko, S. Cahangirov, A. Rubio, Z.J. Lapin, L. Novotny, P. Ayala, T. Pichler, *Nat. Mater.* **15**(6), 634 (2016)
12. K. Kaiser, L.M. Scriven, F. Schulz, P. Gawel, L. Gross, H.L. Anderson, *Science* **365**(6459), 1299 (2019)
13. S. Fang, Y.H. Hu, *Carbon* **171**, 96 (2021)
14. L. Zhang, H. Li, Y.P. Feng, L. Shen, *J. Phys. Chem. Lett.* **11**(7), 2611 (2020)
15. S. Plimpton, *J. Comput. Phys.* **117**(1), 1 (1995)
16. W. Zhu, H. Gong, Y. Han, M. Zhang, A.C.T. van Duin, *J. Phys. Chem. C* **124**(23), 12512 (2020)
17. S. Izrailev, S. Stepaniants, B. Isralewitz, D. Kosztin, H. Lu, F. Molnar, W. Wriggers, K. Schulten, "Steered Molecular Dynamics," in *Computational Molecular Dynamics: Challenges, Methods, Ideas* (Springer, Berlin, 1999), p. 39
18. W. Humphrey, A. Dalke, K. Schulten, *J. Mol. Graph.* **14**(1), 33 (1996)
19. Nanorex, Inc., NanoEngineer-1
20. M. Robinson, N.A. Marks, *Comput. Phys. Commun.* **185**(10), 2519 (2014)
21. R. Mirzaeifar, Z. Qin, M.J. Buehler, *Nanotechnology* **25**(37), 371001 (2014)
22. A.P. Thompson, S.J. Plimpton, W. Mattson, *J. Chem. Phys.* **131**(15), 154107 (2009)
23. A.K. Nair, S.W. Cranford, M.J. Buehler, *Europhys. Lett.* **95**(1), 16002 (2011)
24. M.A. Osman, D. Srivastava, *Nanotechnology* **12**(1), 21 (2001)
25. A. Stukowski, *Model. Simul. Mater. Sci. Eng.* **18**(1), 015012 (2010)
26. F. Müller-Plathe, *J. Chem. Phys.* **106**(14), 6082 (1997)
27. P. Giannozzi, S. Baroni, N. Bonini, M. Calandra, R. Car, C. Cavazzoni, D. Ceresoli, G.L. Chiarotti, M. Cococcioni, I. Dabo, A. Dal Corso, S. de Gironcoli, S. Fabris, G. Fratesi, R. Gebauer, U. Gerstmann, C. Gougoussis, A. Kokalj, M. Lazzeri, L. Martin-Samos, N. Marzari, F. Mauri, R. Mazzarello, S. Paolini, A. Pasquarello, L. Paulatto, C. Sbraccia, S. Scandolo, G. Sclauzero, A.P. Seitsonen, A. Smogunov, P. Umari, R.M. Wentzcovitch, *J. Phys. Condens. Matter* **21**(39), 395502 (2009)
28. P.E. Blöchl, *Phys. Rev. B* **50**(24), 17953 (1994)
29. J.P. Perdew, K. Burke, M. Ernzerhof, *Phys. Rev. Lett.* **77**(18), 3865 (1996)
30. S. Grimme, *J. Comput. Chem.* **27**(15), 1787 (2006)
31. K. Momma, F. Izumi, *J. Appl. Crystallogr.* **41**(3), 653 (2008)
32. M. Alaghemandi, E. Algaer, M.C. Böhm, F. Müller-Plathe, *Nanotechnology* **20**(11), 115704 (2009)
33. R.N. Salaway, L.V. Zhigilei, *Int. J. Heat Mass Transf.* **70**, 954 (2014)
34. L. Lindsay, D.A. Broido, N. Mingo, *Phys. Rev. B* **83**(23), 235428 (2011) □